Mechanical Systems and Signal Processing 200 (2023) 110537

Contents lists available at ScienceDirect

Mechanical Systems and Signal Processing

journal homepage: www.elsevier.com/locate/ymssp

Piezoelectric-shunt-based approach for multi-mode adaptive tuned mass dampers

S. Manzoni [a], M. Berardengo [b,*], F. Boccuto [a], M. Vanali [c]

[a] Politecnico di Milano – Department of Mechanical Engineering, Via La Masa, 1 20156 Milan, Italy
[b] Università degli Studi di Genova - Department of Mechanical, Energy, Management and Transportation Engineering, Via all'Opera Pia, 15A 16145 Genoa, Italy
[c] Università degli Studi di Parma - Department of Engineering and Architecture, Parco Area delle Scienze, 181/A 43124 Parma, Italy

ARTICLE INFO

Communicated by X. Jing

Keywords:
Tuned mass damper
Multi-frequency adaptive tuned mass damper
Multi-mode adaptive tuned mass damper
Adaptive tuned mass damper
Piezoelectric shunt
Negative capacitance

ABSTRACT

This paper deals with the design and development of a multi-frequency adaptive tuned mass damper based on a cantilever beam equipped with shunted piezoelectric elements. It is demonstrated that the device is able to independently shift a number of eigenfrequencies equal to the number of piezoelectric elements and that the use of negative capacitances is able to strongly improve the adaptation capability of the device. Mathematical formulations are provided for linking the values of the capacitances used for shunting the piezoelectric elements and the resulting shifts of the eigenfrequencies, and vice versa. Furthermore, being the negative capacitances based on operational amplifiers, the stability of the electro-mechanical system is investigated, giving rules about the tuning of these negative capacitances. The resulting adaptive tuned mass damper can be fruitfully employed for lowering vibrations of a primary system whose eigenfrequencies undergo different frequency shifts, improving the robustness to possible mistuning of non-adaptive classical tuned mass dampers. All the theoretical outcomes are validated through an experimental campaign with a cantilever beam equipped with two piezoelectric patches.

1. Introduction

The use of tuned mass dampers (TMD) is a widespread approach for attenuating vibrations in structures from small to large [1–5]. Different systems and structures can be currently equipped with TMDs, such as, e.g., buildings [6], hangers [7], cables [8], pipes [9], vehicles [10,11], machine tools [12], floors [13], and many others can be mentioned. The main drawback of these devices is related to the appearance of mistuning when the dynamic features of either the primary system (i.e., the system for which vibrations have to be lowered) or the TMD change due to, e.g., thermal shifts. To solve this problem, active mass dampers (e.g., [14,15]) and adaptive tuned mass dampers (ATMD) have been proposed. ATMDs are devices able to change their dynamic features in response to inputs provided by users/controllers (e.g., [16]). Different physical principles and devices can be employed for developing ATMDs, such as servo-actuators (e.g., [17]), shape memory alloys (e.g., [18–20]), magnetorheological elements (e.g., [21–23]), tensioning systems [24] and pneumatic springs (e.g., [25]); many other physical principles can be used as well (e.g., [26–29]). Among the different approaches for developing ATMDs, the use of piezoelectric elements is promising [30,31] due to the low weight added to the TMD and the easiness of adaptation. It is shown below that the possibility to use piezoelectric elements to develop ATMDs is guaranteed by their capability to act at the same time as sensors and actuators.

* Corresponding author.
E-mail address: marta.berardengo@unige.it (M. Berardengo).

https://doi.org/10.1016/j.ymssp.2023.110537
Received 8 February 2023; Received in revised form 12 June 2023; Accepted 15 June 2023
Available online 1 July 2023

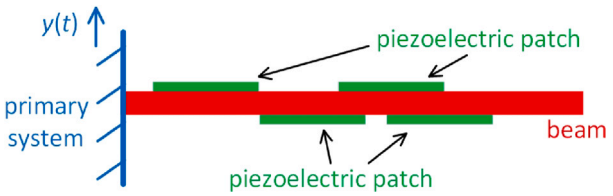

Fig. 1. Cantilever beam equipped with piezoelectric patches and connected to a primary system to be damped.

The way in which piezoelectric elements are used is mainly bonding benders on cantilever beams, where the beam is the main part of the ATMD, and the piezoelectric bender is used to change the dynamics of the beam by means of an electric shunt impedance connected to the bender electrodes (i.e., piezoelectric shunt). Piezoelectric shunt is usually employed for attenuating vibrations of the structure to which piezoelectric elements are attached (e.g., [32–36]). Conversely, here, the aim is to change the dynamics of the cantilever beam by adjusting the shunt impedance, and this allows tuning the beam dynamics to the primary system dynamics. When a mistuning occurs between the primary system and the ATMD, the electric impedance can be changed, e.g., acting on variable resistances, in order to reach again the tuned condition. Different works are available in the literature about the use of this approach for developing ATMDs acting on a single mode of the primary system. Heuss et al. [37] proposed to connect a negative capacitance (NC) to the piezoelectric bender in order to change the value of one eigenfrequency of the ATMD with the purpose to recover changes of the corresponding eigenfrequency of the primary system. Chatziathanasiou et al. [38,39] proposed to shunt an electric impedance made from an inductance and a resistance for controlling a single mode of the primary system (even if the authors show that the device can also be used to damp more than one mode at the same time in [39]), while Yamada and Asami [40] gave formulas for a proper tuning of the TMD dynamic characteristics.

This paper aims at showing how it is possible to develop multi-modal ATMDs able to change independently two or more of its eigenfrequencies in order to reach tuning with the primary system on two or more eigenmodes to be attenuated. The chance to have a single device able to attenuate different eigenmodes of the primary system allows, e.g., saving space and weight and more and more attempts are currently under investigation (e.g. [19,41–43]).

The paper will show that using P piezoelectric benders, each connected with a capacitance (either positive or negative), allows tuning independently P ATMD eigenfrequencies, even if each bender influences the values of all the eigenfrequencies. Furthermore, formulas for the tuning of the capacitances will be provided. The structure of the paper is as follows: Section 2 introduces the model of the ATMD, while Section 3 explains how to carry out the tuning of the capacitances, discusses the stability of the electro-mechanical ATMD and evidences some important considerations about the way to place the benders on the cantilever beam. The same section also discusses some examples and shows how having more piezoelectric elements than modes to be attenuated allows improving the adaptation capability of the ATMD. Finally, Section 4 gives hints about how to tune also the damping of the ATMD, Section 5 discusses the results of an experimental campaign to validate the previous theoretical outcomes and Section 6 briefly explains how to practically build the ATMD.

2. Model of the ATMD

A cantilever beam with P (all the symbols used in the paper are summarised in Appendix A) bonded piezoelectric patches is considered (see Fig. 1). The external disturbance acting on such a system is intended as the displacement $y(t)$ (t is time) of the constraint (i.e., the cantilever beam is constrained at the clamped end to the vibrating primary system). According to Thomas et al. [44], the transverse displacement $U(x,t)$ of the beam (x is the coordinate along the beam length), in a reference system moving with the primary system, can be described through modal coordinates q_i, taking into account modes from the first one to the Nth (i.e., i=1, …, N), with N tending to infinity:

$$U(x,t) = \sum_{i=1}^{N} \Phi_i(x) q_i(t) \tag{1}$$

where Φ_i is the ith eigenmode of the structure normalised to the unit modal mass and with all the patches short-circuited. The use of modal coordinates allows describing the dynamics of the electro-mechanical system (i.e., the cantilever beam with the piezoelectric patches) through N differential equations with the following form:

$$\ddot{q}_i + 2\xi_i\omega_i\dot{q}_i + \omega_i^2 q_i - \sum_{p=1}^{P} \chi_{i,p} V_p = F_i \qquad \forall\, i = 1, \dots, N \tag{2}$$

where ω_i is the ith eigenfrequency of the beam with all the patches short-circuited, ξ_i is the corresponding non-dimensional damping ratio, F_i is the modal forcing term (see, e.g., [20] for its computation) and $\chi_{i,p}$ is a modal coupling coefficient, which is related to the energy transfer between the ith mode shape and the pth piezoelectric patch. Finally, V_p is the voltage across the electrodes of the pth patch. The value of $\chi_{i,p}$ is evaluated with all the patches different from the pth short-circuited and depends on the geometrical, electrical and mechanical characteristics of the piezoelectric element and the beam, as well as on the position of the patch along the beam. The $\chi_{i,p}$ coefficients can be computed with either an analytical model [45] or by a finite element discretisation [44], or also using experimental tests [46,47].

The electrical behaviour of the piezoelectric benders is governed by the following equation [44] (often indicated as sensor equation):

$$C_{\infty,p}V_p - Q_p + \sum_{i=1}^{N} \chi_{i,p} q_i = 0 \qquad \forall\ p = 1, \dots, P \tag{3}$$

where Q_p is the charge in one of the electrodes of the pth patch ($-Q_p$ in the other electrode) and $C_{\infty,p}$ is the blocked capacitance (i.e., with $U(x,t)=0\ \forall\ x$ and, thus, $q_i=0\ \forall\ i$) of the pth bender.

In case of low modal superimposition, a single-degree-of-freedom approximation for the ith mode can be obtained by rearranging Eqs. (2) and (3), respectively, as:

$$\ddot{q}_i + 2\xi_i\omega_i\dot{q}_i + \omega_i^2 q_i - \sum_{p=1}^{P} \chi_{i,p} V_p = F_i \tag{4}$$

$$C_{i,p}V_p - Q_p + \chi_{i,p} q_i = 0 \qquad \forall\ p = 1, \dots, P \tag{5}$$

where $C_{i,p}$ is the modal capacitance of the pth bender at the ith mode. $C_{i,p}$ can be intended as the capacitance of the pth piezoelectric patch at angular frequency values Ω between modes ith and $(i+1)$th (i.e., $\omega_i \ll \Omega \ll \omega_{i+1}$), when all the other patches are short-circuited (thus, neglecting their effect on the trend of the pth capacitance as a function of the frequency). More details about the meaning of the modal capacitance can be found in [47].

Once the modal capacitance $C_{i,p}$ has been introduced, $\chi_{i,p}$ can be also expressed in non-dimensional form as $k_{i,p}$, which is the modal electro-mechanical coupling factor [46] of the ith mode and pth patch:

$$k_{i,p} = \frac{\chi_{i,p}}{\omega_i \sqrt{C_{i,p}}} \tag{6}$$

The value of $k_{i,p}^2$ can be approximated as [46]:

$$k_{i,p}^2 \simeq \frac{(\omega_{i,p}^{\mathrm{oc}})^2 - \omega_i^2}{\omega_i^2} \Rightarrow |k_{i,p}| \simeq \sqrt{\frac{(\omega_{i,p}^{\mathrm{oc}})^2 - \omega_i^2}{\omega_i^2}} \tag{7}$$

where $\omega_{i,p}^{\mathrm{oc}}$ indicates the ith system eigenfrequency when the pth piezoelectric patch is open-circuited while all the others are short-circuited.

According to the convention of sign of V_p and $\dot{Q}_p$ (where $\dot{Q}_p$ is the derivative of Q_p with respect to t, thus an electrical current) in Fig. 2, in case the pth bender is shunted with a capacitance, here referred to as $C_{\mathrm{a},p}$, considering the relationship between V_p and Q_p with this type of shunt impedance, Eq. (5) for the pth bender can be rewritten as:

$$(C_{\mathrm{a},p} + C_{i,p})V_p + \chi_{i,p} q_i = 0 \tag{8}$$

Here, $C_{\mathrm{a},p}$ can be either a positive capacitance (i.e., $C_{\mathrm{a},p} > 0$) or an NC (i.e., $C_{\mathrm{a},p} < 0$).

3. ATMD tuning and stability

This section aims at discussing different aspects which all strictly rely on the model presented in Section 2. More in detail, Section 3.1 discusses how to tune the shunt capacitance values in order to obtain given eigenfrequency values, and vice versa, Section 3.2 discusses the stability of the electro-mechanical system when NCs are used and, finally, Section 3.3 explains how to make the adaptation capability of the ATMD as large as possible.

3.1. Tuning of the shunt capacitances

Assuming the validity of the single-degree-of-freedom approximation (i.e., low modal superimposition), using two piezoelectric patches on the beam (i.e., p=1, 2) for the sake of simplicity, Eq. (4) for the ith mode can be written as:

$$\ddot{q}_i + 2\xi_i\omega_i\dot{q}_i + \omega_i^2 q_i - \chi_{i,p=1}V_{p=1} - \chi_{i,p=2}V_{p=2} = F_i \tag{9}$$

In case each patch is connected to a capacitance, the last equation can be further rearranged by employing Eq. (8):

$$\ddot{q}_i + 2\xi_i\omega_i\dot{q}_i + \left(\omega_i^2 + \frac{\chi_{i,p=1}^2}{C_{\mathrm{a},p=1} + C_{i,p=1}} + \frac{\chi_{i,p=2}^2}{C_{\mathrm{a},p=2} + C_{i,p=2}}\right) q_i = F_i \tag{10}$$

According to Eq. (10), having two patches connected to capacitances, it is possible to achieve new values of eigenfrequencies once the capacitance values have been set. Generally speaking, it is possible to tune n (with $n \leq N$) eigenfrequencies with P patches connected to capacitances, with $P \geq n$. According to Eq. (10), the new values of the eigenfrequencies, referred to as $\omega_{i,\mathrm{new}}$, are linked to the shunt capacitance values through the following equation:

$$\omega_{i,\mathrm{new}}^2 = \omega_i^2 + \frac{\chi_{i,p=1}^2}{C_{\mathrm{a},p=1} + C_{i,p=1}} + \frac{\chi_{i,p=2}^2}{C_{\mathrm{a},p=2} + C_{i,p=2}} \tag{11}$$

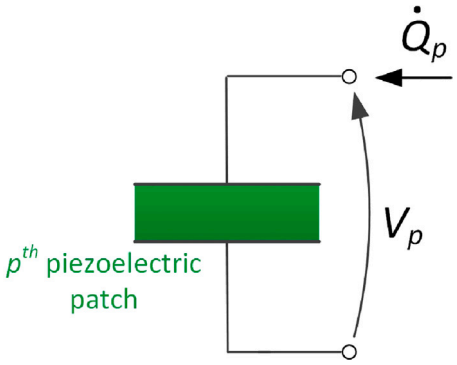

Fig. 2. Convention of sign for the electrical part of the system.

According to Eq. (6), Eq. (11) can be written as:

$$\omega_{i,\text{new}}^2 = \omega_i^2 \left[1 + \frac{k_{i,p=1}^2}{(C_{\text{a},p=1}/C_{i,p=1}) + 1} + \frac{k_{i,p=2}^2}{(C_{\text{a},p=2}/C_{i,p=2}) + 1} \right] \tag{12}$$

Eqs. (11) and (12) are valid for two patches and two shunt capacitances, but can be easily generalised to any other larger number of patches and capacitances. Through simple mathematical treatments and considering two modes (e.g., i=1,2), thus $n = P$, Eq. (11) can be rearranged as:

$$C_{\text{a},p=2} = \frac{-b \pm \sqrt{b^2 - 4ac}}{2a} \tag{13}$$

$$C_{\text{a},p=1} = \frac{(\chi_{i=1,p=1}^2 - \Delta_{i=1} C_{i=1,p=1})(C_{\text{a},p=2} + C_{i=1,p=2}) + \chi_{i=1,p=2}^2 C_{i=1,p=1}}{(C_{\text{a},p=2} + C_{i=1,p=2})\Delta_{i=1} - \chi_{i=1,p=2}^2} \tag{14}$$

with

$$\Delta_{i=1} = \omega_{i=1,\text{new}}^2 - \omega_{i=1}^2 \tag{15}$$

$$\Delta_{i=2} = \omega_{i=2,\text{new}}^2 - \omega_{i=2}^2 \tag{16}$$

$$a = \Delta_{i=2}\lambda - \Delta_{i=1}\chi_{i=2,p=1}^2 \tag{17}$$

$$b = \Delta_{i=2}\left[\lambda(C_{i=1,p=2} + C_{i=2,p=2}) + \chi_{i=1,p=2}^2(C_{i=1,p=1} - C_{i=2,p=1})\right] - \chi_{i=2,p=1}^2\left[\Delta_{i=1}(C_{i=1,p=2} + C_{i=2,p=2}) - \chi_{i=1,p=2}^2\right] - \chi_{i=2,p=2}^2\lambda \tag{18}$$

$$\begin{aligned} c = {} & \Delta_{i=2}C_{i=2,p=2}\left[C_{i=1,p=2}\lambda + \chi_{i=1,p=2}^2(C_{i=1,p=1} - C_{i=2,p=1})\right] - \chi_{i=2,p=1}^2 C_{i=2,p=2}(\Delta_{i=1}C_{i=1,p=2} - \chi_{i=1,p=2}^2) \\ & -\chi_{i=2,p=2}^2\left[C_{i=1,p=2}\lambda + \chi_{i=1,p=2}^2(C_{i=1,p=1} - C_{i=2,p=1})\right] \end{aligned} \tag{19}$$

$$\lambda = \Delta_{i=1}(C_{i=2,p=1} - C_{i=1,p=1}) + \chi_{i=1,p=1}^2 \tag{20}$$

One of the two solutions for $C_{\text{a},p=2}$ in Eq. (13) is either non physical (e.g., complex valued) or unstable (see Section 3.2). Using the physical and stable solution from Eq. (13), $C_{\text{a},p=1}$ can be found with Eq. (14). Therefore, Eqs. (13) and (14) allow finding the shunt capacitance values once the desired values of $\omega_{i=1,\text{new}}$ and $\omega_{i=2,\text{new}}$ have been set.

The formulas in Eqs. (12), (13) and (14) allow linking the new (and desired) values of the eigenfrequencies to the values of the shunt capacitances. This poses the foundation for making the TMD adaptive by changing the values of the shunt capacitances. Obviously, one should also set the initial values of ω_i according to the considered eigenfrequency values of the primary system. This point is not treated in this paper because there are different degrees of freedom for properly setting the values of ω_i whose effects are already described in the literature, such as, e.g.:

- changes of beam length and thickness [48];
- changes of the position of the P patches along the beam, as well as of their size and mechanical characteristics [45]. Moreover, further in the manuscript, it is shown that the use of more patches than modes to be tuned allows widening the adaptation range of the ATMD. This increased adaptation range can also be exploited to the aim of the initial tuning of the ATMD;
- addition of concentrated masses in given locations x of the beam (e.g., [49,50]). As an example, Wu and Lin shows in [49] that the eigenfrequency ratio between the first and the second modes of a cantilever beam can range from approximately 4 to 7 with a single mass properly placed along the beam (i.e., a mass has different effects on the different eigenfrequency values according to its position);

- change of beam constraint type. As an example, passing from a cantilever beam to a clamped–clamped beam allows reducing the ratio between the first and the second eigenfrequency values approximately from 6 to 2.7 [51]. The eigenfrequencies of the clamped-clamped beam can be then tuned using the same approach described here for the cantilever beam and all the formulations provided in the paper are valid also in this further case;
- use of a different type of system for building the ATMD. As an example, one could build a two degree-of-freedom system equipped with two piezoelectric stacks (see, e.g., [52] for TMDs relying on piezoelectric stacks). This new layout of the ATMD can be still used for multi-frequency adaptation. as described in this paper.

3.2. Stability of the electro-mechanical system

NCs do not exist in nature and are built with circuits based on operational amplifiers [53]. Therefore, when they are added as shunt impedances, the stability of the electro-mechanical system must be studied since instability could arise due to the active nature of NC circuits [54].

To study the electro-mechanical system stability, the characteristic polynomial of the system is considered. Using again the example where two piezoelectric elements are placed on the hosting beam to tune two eigenfrequencies of the ATMD, according to Eq. (10), this polynomial can be written for the ith mode as:

$$A_i \mathrm{s}^2 + B_i \mathrm{s} + D_i = 0 \tag{21}$$

where s is the Laplace operator and:

$$A_i = (C_{\mathrm{a},p=1} + C_{i,p=1})(C_{\mathrm{a},p=2} + C_{i,p=2}) \tag{22}$$

$$B_i = 2\xi_i \omega_i A_i \tag{23}$$

$$D_i = \chi^2_{i,p=1}(C_{\mathrm{a},p=2} + C_{i,p=2}) + \chi^2_{i,p=2}(C_{\mathrm{a},p=1} + C_{i,p=1}) + \omega_i^2 A_i \tag{24}$$

In investigating stability, the starting points considered here are the stability conditions when a single piezoelectric element is connected to an NC and the other is short-circuited. Indeed, also configurations with a single NC will be considered for the ATMD (see further in the paper). Being $C_{0,p}$ the value of the piezoelectric capacitance at the null frequency for the pth piezoelectric element and being valid the following relationship [55]:

$$C_{0,p} = C_{i=1,p}(1 + k^2_{i=1,p}) \geq C_{i,p} \geq C_{i+1,p} \geq \cdots \geq C_{i+10,p} \geq \cdots \geq C_{\infty,p} \tag{25}$$

then, according to [54,55], these stability conditions are $C_{\mathrm{a},p} > -C_{i,p}$ and $C_{\mathrm{a},p} < -C_{i-1,p}$ when considering only the ith mode, and $C_{\mathrm{a},p} > -C_{\infty,p}$ and $C_{\mathrm{a},p} < -C_{0,p}$ for the whole system (i.e., considering all the modes, which means that these are the actual stability conditions of the electro-mechanical system).

To assure stability of the ith mode, A_i, B_i and D_i must have the same sign. For the stability of the whole system, all the modes must be stable. The global stability conditions are provided here below and they are discussed in detail in Appendix B.

There are four different possible stable configurations. The first stable configuration, named conf1, is:

$$C_{\mathrm{a},p=1} < -C_{0,p=1}, \quad C_{\mathrm{a},p=2} < -C_{i=1,p=2}(1 + k^2_{i=1,p=2} X_{i=1,p=1}) \tag{26}$$

where:

$$X_{i=1,p=1} = \frac{C_{\mathrm{a},p=1} + C_{i=1,p=1}}{C_{\mathrm{a},p=1} + C_{0,p=1}} = \frac{C_{\mathrm{a},p=1} + C_{i=1,p=1}}{C_{\mathrm{a},p=1} + C_{i=1,p=1}(1 + k^2_{i=1,p=1})} \tag{27}$$

and $C_{0,p}$, as mentioned, is the value of the piezoelectric capacitance at the null frequency for the pth piezoelectric element and, according to [55], $C_{0,p} = C_{i=1,p}(1 + k^2_{i=1,p})$.

It is worth noticing that a condition equivalent to Eq. (26) is the following:

$$C_{\mathrm{a},p=2} < -C_{0,p=2}, \quad C_{\mathrm{a},p=1} < -C_{i=1,p=1}(1 + k^2_{i=1,p=1} X_{i=1,p=2}) \tag{28}$$

The second possible configuration for stability, named conf2, is:

$$C_{\mathrm{a},p=1} > -C_{\infty,p=1}, \quad C_{\mathrm{a},p=2} > -C_{\infty,p=2} \tag{29}$$

Then, the third stable configuration, conf3, is:

$$C_{\mathrm{a},p=1} > -C_{\infty,p=1}, \quad C_{\mathrm{a},p=2} < -C_{0,p=2} \tag{30}$$

and the fourth, conf4, is:

$$C_{\mathrm{a},p=1} < -C_{0,p=1}, \quad C_{\mathrm{a},p=2} > -C_{\infty,p=2} \tag{31}$$

Table 1
Values of $|k_{i,p}|$ for the simulations aimed at showing their effects on the achievable r_i values.

Case ID	$\lvert k_{i=1,p=1}\rvert$	$\lvert k_{i=1,p=2}\rvert$	$\lvert k_{i=2,p=1}\rvert$	$\lvert k_{i=2,p=2}\rvert$
case 1	0.02	0.02	0.02	0.02
case 2	0.2	0.02	0.02	0.2
case 3	0.2	0.2	0.2	0.2

Table 2
Parameter values for the simulations aimed at showing the effect of α_p and β_p on the achievable r_i values.

$\lvert k_{i=1,p=1}\rvert$	$\lvert k_{i=1,p=2}\rvert$	$\lvert k_{i=2,p=1}\rvert$	$\lvert k_{i=2,p=2}\rvert$	$C_{i=1,p=1}$ [nF]	$C_{i=1,p=2}$ [nF]	$C_{\infty,p=1}$ [nF]	$C_{\infty,p=2}$ [nF]
0.244	0.096	0.072	0.184	79.82	83.66	57.03	58.71

Table 3
Values of $|k_{i,p}|$ for the simulations aimed at comparing the cases with 2 and 3 patches.

Case	$\lvert k_{i=1,p=1}\rvert$	$\lvert k_{i=1,p=2}\rvert$	$\lvert k_{i=1,p=3}\rvert$	$\lvert k_{i=2,p=1}\rvert$	$\lvert k_{i=2,p=2}\rvert$	$\lvert k_{i=2,p=3}\rvert$
2 patches	0.2	0.02	–	0.02	0.2	–
3 patches	0.2	0.02	0.1	0.02	0.2	0.1

3.3. Adaptation capability

Sections 3.1 and 3.2 have explained how to tune the eigenfrequencies of the coupled system and which are the stability thresholds in case NCs are used for shunting the piezoelectric patches. This section is aimed at discussing how it is possible to enlarge the adaptation capability of the ATMD and which are the main parameters involved in the definition of the adaptation range.

Observing Eq. (12), one can infer that the parameters governing the shift of the eigenfrequencies are the ratios between the shunt capacitances and the modal capacitances of the considered mode, as well as the values of the modal electro-mechanical coupling factors $k_{i,p}$. The tuning of the capacitance ratios is related to the choice of the shunt capacitance values and it is observed that the closer the ratios $C_{a,p}/C_{i,p}$ are to -1, the larger the shift of ω_i is, and that $C_{a,p}/C_{i,p}$ cannot be set very close to -1 because of the stability limits (see Eqs. (25), (26) and (28) to (31)).

Considering the role of $k_{i,p}$, in case both $k^2_{i,p=1}$ and $k^2_{i,p=2}$ are characterised by small values for the ith mode, it is necessary to have ratios $C_{a,p}/C_{i,p}$ as close as possible to -1 for obtaining large shifts of the value of ω_i. This implies that NCs must be used and their values must be as close as possible to the stability thresholds described in Section 3.2. Conversely, in case the values of $k^2_{i,p}$ are large (e.g., larger than 0.01), it is possible to produce large shifts of ω_i without pushing the values of the NCs too close to the stability thresholds (i.e., $C_{a,p}/C_{i,p}$ ratios far from -1). To obtain this goal, one might look for bender features which enlarge at best the values of both $k^2_{i,p=1}$ and $k^2_{i,p=2}$. This can be obtained by properly choosing the material of the patches, their size compared to that of the cantilever beam and their position along the beam [45,56]. However, in case more than one mode must be shifted (as in the example discussed here with i=1,2), it is not possible to optimise the features of the piezoelectric patches for more than one mode. Indeed, as explained in [45], for a given patch p, when its features are optimised for controlling a given mode, e.g., i=1 (i.e., obtaining the maximum possible value of $k^2_{i=1,p}$), then these feature values are not optimal for the other mode, i=2.

A straightforward approach to the problem is to optimise the features of one patch for making the corresponding $k^2_{i,p}$ value as high as possible for one of the two modes, and then choose the characteristics of the second patch for maximising the corresponding $k^2_{i,p}$ value for the other mode. As an example, it is possible to choose the features of patch 1 for maximising $k^2_{i=1,p=1}$ and the features of patch 2 for maximising $k^2_{i=2,p=2}$. This implies that, for each of the two modes, at least one $k^2_{i,p}$ value in Eq. (12) is large.

To quantify the capability of adaptation, the following index is used:

$$r_i = \omega_{i,\mathrm{new}}/\omega_i \tag{32}$$

Fig. 3 shows the values of $r_{i=1}$ and $r_{i=2}$ for different combinations of the four $k^2_{i,p}$ values involved in the example: $k^2_{i=1,p=1}$, $k^2_{i=1,p=2}$, $k^2_{i=2,p=1}$ and $k^2_{i=2,p=2}$. For obtaining the plots, all the stability configurations discussed above (i.e., from conf1 to conf4) have been considered and the values of the two shunt capacitances $C_{a,p}$ have been changed following the procedure below:

1. the values of $C_{a,p=1}$ and $C_{a,p=2}$ are set to a very high value (e.g., 1 F) and r_i is calculated for both the considered modes;
2. the value of $C_{a,p=2}$ is decreased step by step using a logarithmic law until $C_{a,p=2}$ reaches negative values not far from the instability limit $-C_{\infty,p=2}$ (see Eq. (29)). In this example, the decrease of $C_{a,p=2}$ is stopped when its value reaches $-C_{\infty,p=2}/3$ to stay far from instability. For each of the considered values of $-C_{a,p=2}$, corresponding r_i values are calculated;
3. the other stability range for $C_{a,p=2}$ is then considered, still keeping $-C_{a,p=1}$ at the initial value. This further stability range is given in Eq. (30). In this example, the values of $C_{a,p=2}$ are set between $-3C_{0,p=2}$ and a very large and negative value (e.g., -1 F) (again a logarithmic step is used);

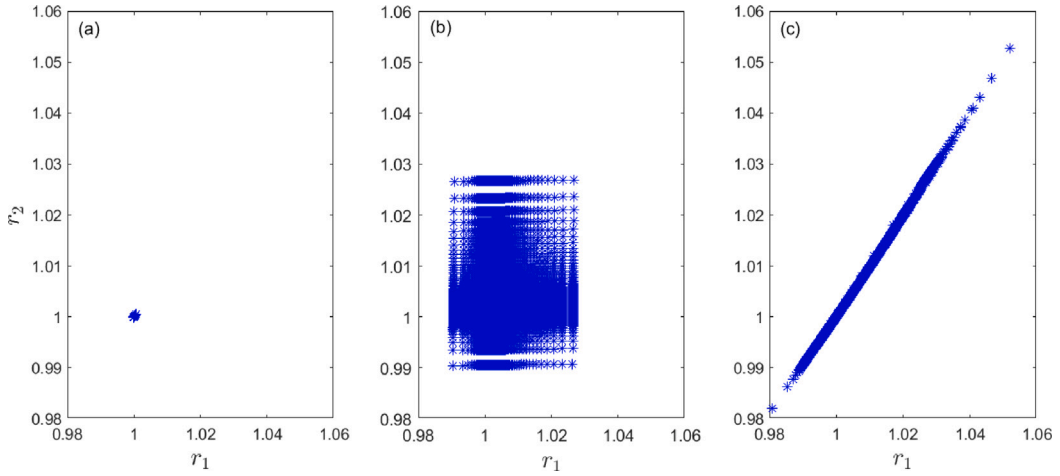

Fig. 3. Resulting (r_1, r_2) plots for case 1 (a), case 2 (b) and case 3 (c) of Table 1. Here, $C_{\infty,p=1} = C_{\infty,p=2} = 60$ nF and $C_{i=1,p=1} = C_{i=1,p=2} = 80$ nF.

4. Points 2 and 3 of this list are repeated for decreased values of $C_{\mathrm{a},p=1}$. To fulfil the stability conditions in Eqs. (29) and (30), the decrease of $C_{\mathrm{a},p=1}$ is stopped at $-C_{\infty,p=1}/3$;
5. The whole procedure above is repeated for the other stability configurations (i.e., considering Eqs. (26) and (31)). The ranges used for the two capacitance values are:
   - between -1 F and $-3C_{0,p=1}$ for $C_{\mathrm{a},p=1}$ and between -1 F and $-3C_{i=1,p=2}(1 + k^2_{i=1,p=2}X_{i=1,p=1})$ for $C_{\mathrm{a},p=2}$ (see Eq. (26));
   - between -1 F and $-3C_{0,p=1}$ for $C_{\mathrm{a},p=1}$ and between $-C_{\infty,p=2}/3$ and 1 F for $C_{\mathrm{a},p=2}$ (see Eq. (31)).

This procedure allows deriving the clouds of points shown in the plots of Fig. 3. Each plot is obtained for different values of $|k_{i=1,p=1}|$, $|k_{i=1,p=2}|$, $|k_{i=2,p=1}|$ and $|k_{i=2,p=2}|$, as described in Table 1. When, for a given mode, both the corresponding $|k_{i,p}|$ values are small (see case 1 in Table 1 and plot (a)), the corresponding achievable r_i range is limited or even negligible. Conversely, when all the $|k_{i,p}|$ values are large enough, the obtained cloud of points is large (case 3 in Table 1 and plot (c)). However, for the case considered in plot (c), it is not possible to have a certain degree of independence in moving separately the two considered eigenfrequencies. Indeed, large shifts of ω_1 (i.e., values of r_1 largely different from 1) always correspond to large shifts of ω_2 (i.e., values of r_2 largely different from 1). The shape of the cloud in plot (c) is not desiderable because, with this layout, the ATMD is not able to change the two eigenfrequencies independently. Finally, plot (b), corresponding to case 2 in Table 1, evidences that, in case one $|k_{i,p}|$ value is high enough for one mode and small for the other, and the opposite occurs for the other mode (see case 2 in Table 1), the obtained plot is large and approximates a square. Therefore, under a practical point of view, to obtain a large range of adaptation and a given level of independence in moving the eigenfrequencies (i.e., large and squared clouds), it is needed to place one piezoelectric element such that the $|k_{i,p}|$ value is large enough (e.g., larger than 0.1) for one mode while a small value of $|k_{i,p}|$ must be obtained for the other mode, and to do the opposite for the other piezoelectric patch. It is noticed that the blank spaces in Fig. 3 are only related to a non sufficiently small step for the $C_{\mathrm{a},p}$ values used in the simulations. With a smaller step, these spaces would be filled in. This was not carried out here because it would have significantly increased the computational burden without any advantage.

It is now useful to introduce two further parameters: α_p and β_p. They express in a normalised way how much the $C_{\mathrm{a},p}$ values are far from the stability limits. More in detail, α_p is used when the corresponding $C_{\mathrm{a},p}$ value is lower than $-C_{0,p}$ and β_p is used when the corresponding $C_{\mathrm{a},p}$ value is higher than $-C_{\infty,p}$ (see the stability conditions in Eqs. (26) and (28) to (31), as well as Eq. (25)):

$$\alpha_p = -C_{0,p}/C_{\mathrm{a},p}, \quad C_{\mathrm{a},p} < -C_{0,p} \tag{33}$$

$$\beta_p = C_{\mathrm{a},p}/(-C_{\infty,p}), \quad C_{\mathrm{a},p} > -C_{\infty,p} \tag{34}$$

With these definitions, stability is assured when these two parameters are smaller than 1. Actually, when conf1 is used, the actual stability limit is different from $-C_{0,p}$ for one of the two patches (see Eqs. (26) and (28)). However, for the sake of simplicity, here either $X_{i=1,p=1}$ or $X_{i=1,p=2}$ are considered as close enough to 1 that the stability limits can be approximated to $-C_{0,p}$ for both the NCs connected to the patches.

Fig. 4 shows how different values of α_p and β_p are able to change the values of r_i. The parameter values of the system considered are gathered in Table 2 and have been chosen close to the nominal values of the experimental set-up used in Section 5 for validating the theoretical results described in the manuscript. The figure shows the adaptation area for different levels of stability margins. The inner area of each plot, thus, represents the possible values of r_i with given maximum values of α_p and β_p. Thus, as an example, for the area related to the solid blue line, the largest value used for $\alpha_{p=1}$, $\alpha_{p=2}$, $\beta_{p=1}$ and $\beta_{p=2}$ is 0.8. Obviously, the closer the NCs are to the stability limits (i.e., α_p and β_p closer to 1), the larger these areas are. Nevertheless, even without staying close to instability,

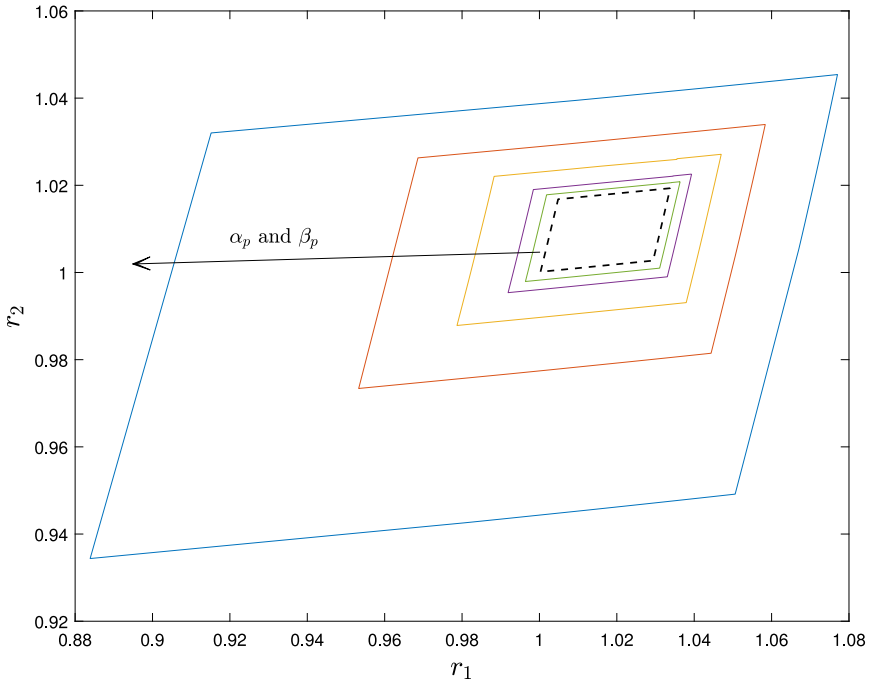

Fig. 4. Resulting (r_1, r_2) areas for different maximum values of α_p and β_p for the system of Table 2. Here, the maximum values for α_p and β_p are: 0.1, 0.2, 0.4, 0.6, 0.8 (solid lines in the plot). Furthermore, the case where only positive capacitances are used for shunting the two piezoelectric patches (i.e., $\beta_{p=1} \leq 0$ and $\beta_{p=2} \leq 0$) is also shown by means of a dashed line.

significantly large areas are obtained. Indeed, the area related to 0.6 as largest value of α_p and β_p shows that ω_1 can be changed of approximately 8% and ω_2 of about 5%, as an example. The areas related to different values of α_p and β_p are also compared to the area related to the sole use of positive shunt capacitances (dashed line in the figure), which corresponds having $\beta_{p=1} \leq 0$ and $\beta_{p=2} \leq 0$. It comes out that using NCs allows significantly enlarging the adaptation area.

Furthermore, to have a clear evidence of how different combinations of the shunt capacitances lead to cover different areas in the (r_1, r_2) plot, Fig. 5 is presented and it is related to the system of Table 2 and largest possible values of α_p and β_p equal to 2/3, chosen as an example.

It is noticed that if one would like to increase the adaptation range of only either the first or the second eigenfrequency without changing the maximum α_p and β_p values, this target can be obtained by properly choosing the position of the patches, as well as their features (e.g., size), in order to increase $k^2_{i=1,p=1} + k^2_{i=1,p=2}$ for the first mode or $k^2_{i=2,p=1} + k^2_{i=2,p=2}$ for the second mode (see Eq. (12)).

Finally, a last example is discussed through the simulation results presented in Fig. 6. Here, a further patch is added (see Table 3) and the two areas shown in the figure evidence that using more patches than modes to be controlled allows making wider the adaptation area compared to the case in which a number of patches equal to the number of modes to be controlled is employed. In this example, the simulated results have been obtained by using Eq. (12) for the case of two patches and a modified version of the same equation for three patches. The modification consists in the addition of a further term related to the third piezoelectric element with the same mathematical form of the contributions of the other two patches. In this simulation, for all the patches, the $C_{a,p}$ value closest to instability is $-3C_{0,p}$ when $C_{a,p} < -C_{0,p}$ and $-C_{\infty,p}/3$ when $C_{a,p} > -C_{\infty,p}$.

To summarise, the adaptation area can be enlarged by:

- increasing the values of $|k_{i,p}|$ by properly choosing size, material and position of the piezoelectric elements;
- using values of α_p and β_p closer to 1;
- using more piezoelectric patches than modes to be tuned.

These three actions can be carried out together, thus leading to a more effective action on the adaptation area.

4. Tuning of the damping

This section briefly introduces how it is possible to adapt also the damping of the ATMD. Two main possibilities are discussed here. The first one is related to the use of non-contact devices such as, e.g., eddy current devices [57] and electromagnetic shunt dampers [58]. This solution can be easily adopted and only requires to have a part of the damping system directly connected to the

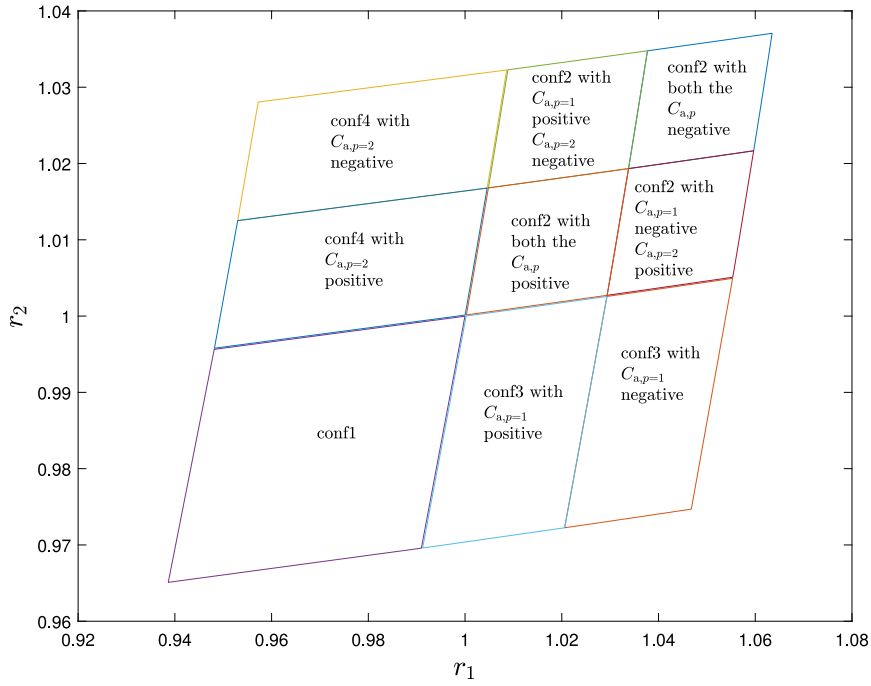

Fig. 5. Resulting (r_1, r_2) areas for different combinations of the shunt capacitances for the system of Table 2 and maximum values of α_p and β_p equal to 2/3.

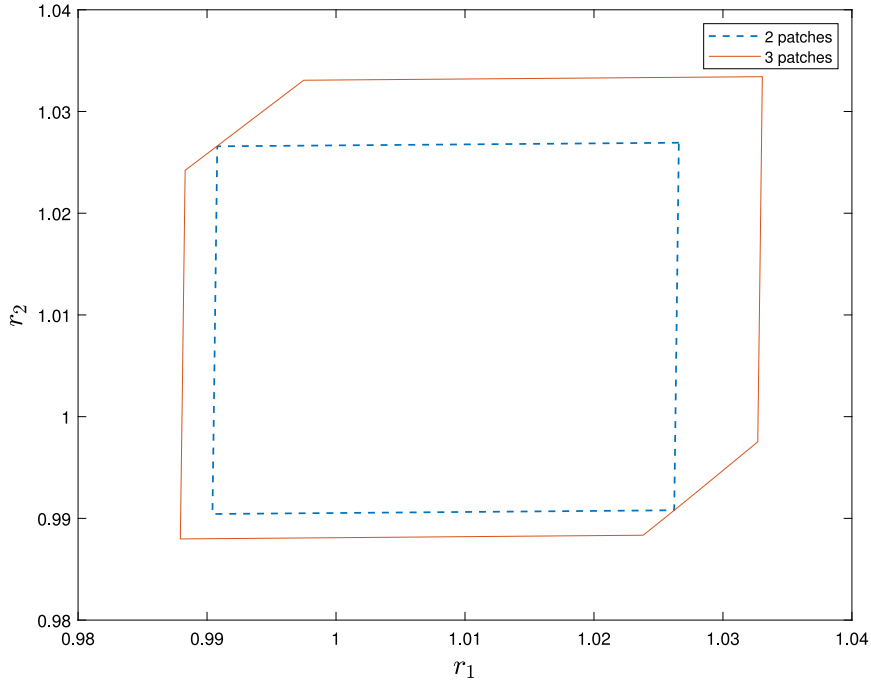

Fig. 6. Resulting (r_1, r_2) areas for the cases in Table 3. Here, $C_{\infty,p=1} = C_{\infty,p=2} = C_{\infty,p=3} = 60$ nF and $C_{i=1,p=1} = C_{i=1,p=2} = C_{i=1,p=3} = 80$ nF.

cantilever beam of the ATMD, and another one grounded/connected to the primary system. As an example, in the case related to electromagnetic shunt dampers, a permanent magnet can be mechanically connected to the vibrating cantilever beam and a coil, shunted with a proper electric impedance, can be grounded/connected to the primary system.

The second possibility for adapting damping is based on an approach which does not require to add any mechanical element to the ATMD. The only addition needed is related to electric resistances in the shunt circuit of the piezoelectric patches. This means that

Table 4
Nominal values of ω_1 and ω_2 identified by means of experimental modal analysis.

Mode i	$\omega_i/(2\pi)$ [Hz]
1	22.24
2	124.51

Table 5
$C_{i=1,p}$ and $C_{\infty,p}$ values estimated experimentally.

Patch p	$C_{i=1,p}$ [nF]	$C_{\infty,p}$ [nF]
1	79.82	57.03
2	83.66	58.71

Table 6
Values of $|k_{i,p}|$, $C_{a,p}$, α_p and β_p for all the tests.

Test ID	$\lvert k_{i=1,p=1}\rvert$	$\lvert k_{i=1,p=2}\rvert$	$\lvert k_{i=2,p=1}\rvert$	$\lvert k_{i=2,p=2}\rvert$	$C_{a,p=1}$ [nF]	$C_{a,p=2}$ [nF]	$\alpha_{p=1}$ or $\beta_{p=1}$	$\alpha_{p=2}$ or $\beta_{p=2}$
T1	0.242	0.090	0.057	0.188	−35.0	−538.6	$\beta_{p=1}$=0.61	$\alpha_{p=2}$=0.16
T2	0.242	0.090	0.057	0.188	64.8	−104.7	$\beta_{p=1}$=−1.14	$\alpha_{p=2}$=0.81
T3	0.242	0.094	0.071	0.184	−39.6	−36.5	$\beta_{p=1}$=0.69	$\beta_{p=2}$=0.62
T4	0.242	0.094	0.066	0.186	−39.4	−119.7	$\beta_{p=1}$=0.69	$\alpha_{p=2}$=0.70
T5	0.242	0.094	0.066	0.186	−114.0	−38.6	$\alpha_{p=1}$=0.74	$\beta_{p=2}$=0.66
T6	0.242	0.090	0.057	0.188	−114.0	−119.1	$\alpha_{p=1}$=0.74	$\alpha_{p=2}$=0.71
T7	0.242	0.094	0.071	0.184	−25.9	−33.5	$\beta_{p=1}$=0.45	$\beta_{p=2}$=0.57
T8	0.244	0.096	0.072	0.184	55.7	−36.0	$\beta_{p=1}$=−0.98	$\beta_{p=2}$=0.61
T9	0.242	0.094	0.066	0.186	−164.1	−38.7	$\alpha_{p=1}$=0.52	$\beta_{p=2}$=0.66
T10	0.244	0.096	0.072	0.184	−118.9	−28.8	$\alpha_{p=1}$=0.71	$\beta_{p=2}$=0.49
T11	0.242	0.090	0.057	0.188	−121.6	42.4	$\alpha_{p=1}$=0.69	$\beta_{p=2}$=−0.72
T12	0.242	0.094	0.066	0.186	−128.3	−146.7	$\alpha_{p=1}$=0.66	$\alpha_{p=2}$=0.58
T13	0.242	0.094	0.066	0.186	−32.0	−127.3	$\beta_{p=1}$=0.56	$\alpha_{p=2}$=0.66
T14	0.244	0.096	0.072	0.184	29.8	15.7	$\beta_{p=1}$=−0.52	$\beta_{p=2}$=−0.27
T15	0.242	0.090	0.057	0.188	−159.3	−166.6	$\alpha_{p=1}$=0.53	$\alpha_{p=2}$=0.51

the pth piezoelectric patch is shunted with either the series or the parallel of a capacitance $C_{a,p}$ and a resistance R_p. The resistances allow changing the damping of the considered modes [46]. In future works, the approach for tuning together the capacitances and the resistances of the shunt impedances will be developed and presented.

5. Experiments

This section discusses the experimental campaign carried out for validating the previous theoretical results.

The set-up used for the tests is a stainless steel cantilever beam (length 210 mm, width 30.5 mm, thickness 1 mm) with two piezoelectric patches (material PIC 151, length 70 mm, width 30 mm, thickness 0.5 mm) bonded at the clamped end and at 70 mm from the constraint, respectively (see Fig. 7). The excitement provided to the beam was obtained by a contact-less device composed by a permanent magnet bonded close to the beam tip and a coil where electrical current flows. The interaction between the magnetic fields produced by the current flowing in the coil and by the permanent magnet allowed producing a forcing on the beam. The force exerted on the beam is considered as proportional to the current flowing in the coil [59]; this current was thus measured with a current clamp to estimate the forcing term. The excitement provided to the beam was of random nature in the frequency range of the first two resonances (see Table 4). The vibration response of the beam was measured by means of a laser Doppler velocimeter focused close to the beam tip.

Table 4 gathers the values of ω_1 and ω_2 estimated experimentally with the two piezoelectric patches short-circuited. The $C_{i=1,p}$ values were obtained by measuring the piezoelectric capacitances as function of frequency with an impedance analyser and fitting their experimental trends [47]. The values of $C_{\infty,p}$ were instead estimated measuring the value of the capacitance of the piezoelectric patches at very high frequency (i.e., 100 kHz). All these values are reported in Table 5. The values of $C_{i=2,p}$ were found by estimating $k^2_{i=2,p}$ values and using Eq. (B.6). Moreover, the $k^2_{i,p}$ values were estimated by means of Eq. (7), It is important to notice that the values of ω_i and $|k_{i,p}|$ were estimated every time before each of the tests presented below (see Table 6 for the $|k_{i,p}|$ values). Indeed, since the tests lasted different days, the mentioned parameters underwent slight shifts.

Tests with different values of the pairs $(C_{a,p=1}, C_{a,p=2})$ were carried out. In the tests where the $C_{a,p}$ values were negative and lower than $-C_{0,p}$ (see the stability limits), the corresponding NCs were built using the electrical schematic in Fig. 8a. This layout, often used in practice [60], is actually the parallel between an NC and a resistance R_{eq} [55]:

$$-C_a = -\hat{C}(R_{e,2}/R_{e,1}) \tag{35}$$

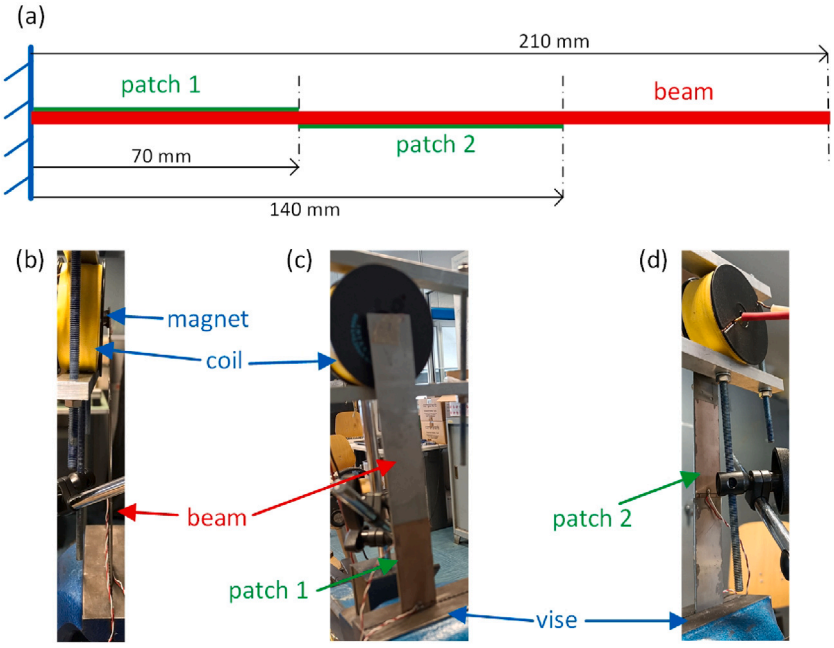

Fig. 7. Set-up used for the tests: schematic (a), side view (b) and detail of the two patches (c, d).

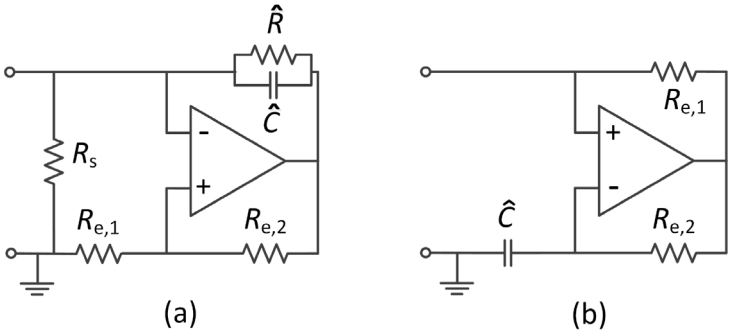

Fig. 8. NC layouts used in this work.

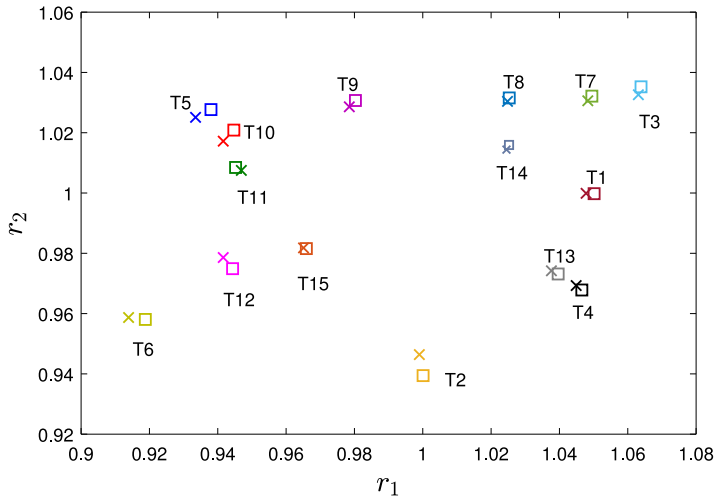

Fig. 9. Experimental (x) and theoretical (□) results in terms of r_1 and r_2 values for the tests of Table 6.

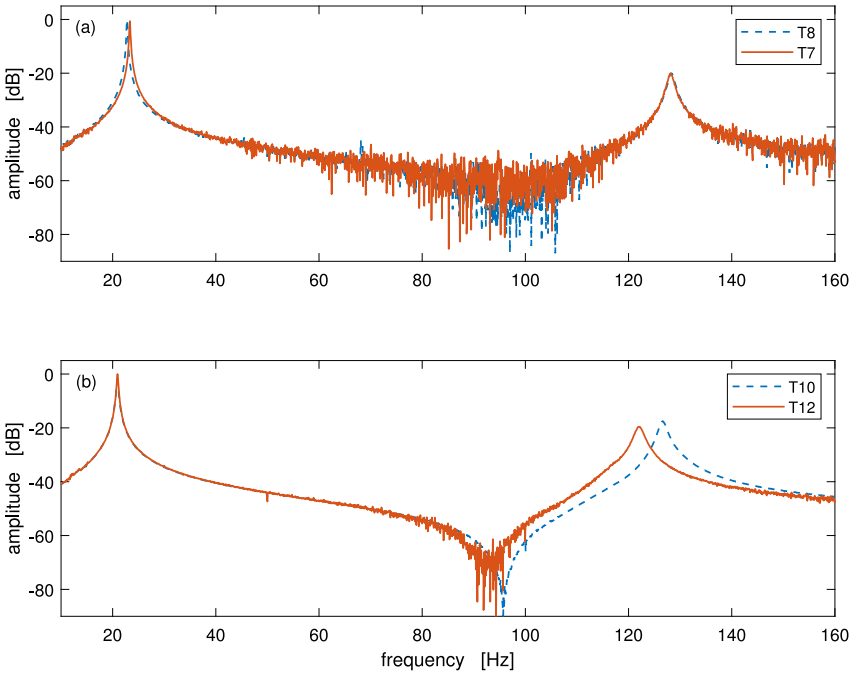

Fig. 10. Experimental FRF amplitudes in terms of velocity/force for T7 and T8 (a) and for T10 and T12 (see Table 6) (b). 0 dB corresponds to the maximum of each plot.

$$R_{\mathrm{eq}} = \tilde{R} R_{\mathrm{s}} / (\tilde{R} - R_{\mathrm{s}}) \tag{36}$$

with

$$\tilde{R} = \hat{R}(R_{\mathrm{e},1} / R_{\mathrm{e},2}) \tag{37}$$

To compensate the additional effect of R_{eq}, its value was set largely negative (i.e., around -75 MΩ) by properly tuning the value of R_{s} [55]. This allowed approximating the behaviour of a pure NC with value as in Eq. (35). Conversely, when the $C_{\mathrm{a},p}$ values were negative and higher than $-C_{\infty,p}$, the NC configuration used was simpler and it is presented in Fig. 8b. This layout is a pure NC given as in Eq. (35).

The values used in the tests for the $C_{\mathrm{a},p}$ capacitances are gathered in Table 6. Fig. 9 reports the comparison between model and experiment results in terms of r_1 and r_2 values for all the tests. The theoretical results have been calculated by means of Eq. (12). The comparison is always satisfactory and the differences between experimental and model results slightly increase only for large values of r_i. This is due to the uncertainty affecting the estimates of the input parameters (e.g., the values of $C_{i,p}$, $k_{i,p}^2$) and non-ideality of the behaviour of the operational amplifiers used to build the NCs. These factors generate slight differences between model and experimental results, which become more and more evident when the NCs are closer and closer to instability limits because, in these cases, the NCs have larger and larger effects. It is noticed that ω_1 has been modified by a total of approximately 14% in the experiments (see Fig. 9), while ω_2 by a total of about 8%, which are remarkable shifts, also considering that they can be obtained independently one from the other. To further increase these shifts, it is possible to act as described in Section 3.3.

Other interesting plots are those provided in Fig. 10, where the ATMD Frequency Response Functions (FRF) are provided for some tests of Table 6. In plot (a), the two FRFs considered show that it is possible to change ω_1 while keeping the value of ω_2 fixed. The opposite case is shown in plot (b). This proves that this ATMD is able to independently shift two (or more) eigenfrequencies at the same time and, therefore, it is able to follow different changes of two (or more) eigenfrequencies of the primary system.

6. Practical aspects in the realisation of the ATMD

This section briefly explains how it is possible to build the ATMD and underlines some aspects related to its implementation.

The way in which the TMD is made adaptive is the connection of a capacitance to each piezoelectric patch. The capacitance can be either positive or negative and its value must be adjustable in real time so that, when a change of the primary system eigenfrequencies occurs (e.g., due a thermal variation), the tuned condition can be reached again, maximising the effect of the ATMD. This requires having the possibility to connect/disconnect either a negative or a positive capacitance. This can be easily

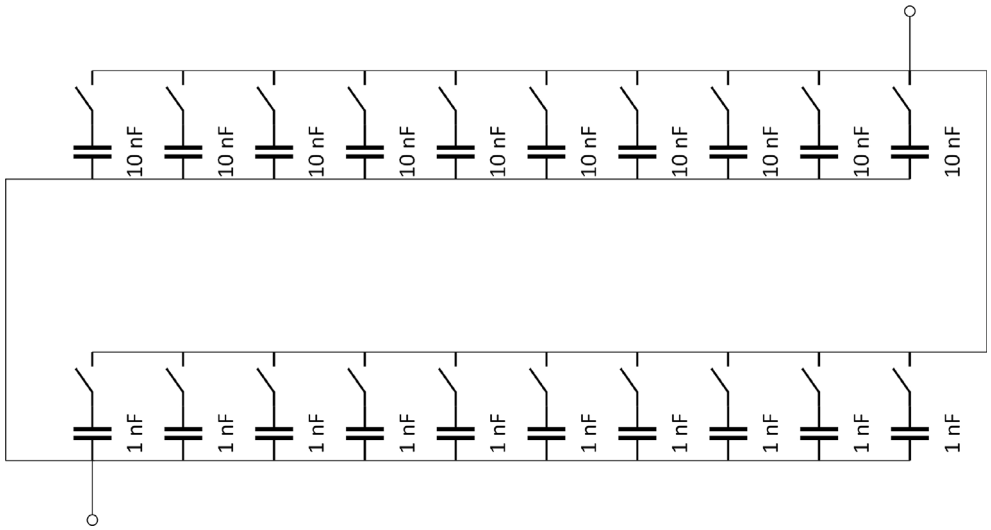

Fig. 11. Possible layout based on switches for remote control of positive shunt capacitances. Each layer of capacitances is made from ten elements.

obtained by using remote switches for connecting/disconnecting the two capacitances to the corresponding patch. This obviously requires to have a real-time controller able to manage the change of connection configuration.

Furthermore, both the positive and negative capacitances must be adjustable, meaning that their values have to be changed when needed. For the NC, this is easily obtained by using digital potentiometers. As an example, the constant resistance $R_{e,1}$ in Fig. 8b can be substituted by a digital potentiometer adjustable by the real-time controller. As for the positive capacitance, it can be built using a layout like that in Fig. 11 based on switches controlled by the real-time unit. This layout only requires to set the order of magnitude of the highest and lowest capacitances according to the highest values required and to the accuracy needed for the final resulting value, respectively, with the possibility of adding further layers composed by ten elements, compared to the case of Fig. 11.

Some further aspects have to be considered:

- the first one is related to the fact that a feedback sensor is needed in order to identify whether the ATMD is properly tuned to the primary system or not. When mistuning occurs, the real-time controller must adjust the shunt impedance according to the mistuning identified through the feedback sensor. This feedback sensor can be, as an example, an accelerometer directly attached to the cantilever beam of the ATMD. Approaches for successfully carrying out the mentioned identification and adaptation are already available in the literature (e.g., [57,61]);
- the second point is related to the fact that, in order to increase the control action on the primary system, the ATMD can be equipped with an additional mass placed at its tip to increase the force it can provide (e.g., [20]);
- when using an ATMD for a multi-mode problem, the control performances on different modes are function of the eigenvector components of the primary system at the connection point (i.e., the point where the ATMD is linked to the primary system). Furthermore, in the case the ATMD is based on a continuous system (e.g., a cantilever beam like in the present case), the force exerted by the ATMD on the primary system depends on the mode shapes of the ATMD (see, e.g., [20] for the forces exerted by a cantilever beam). Therefore, when employing an ATMD like that presented here, one has to investigate where to link the ATMD to the primary system and which modes of the ATMD have to be considered for the control action in order to check if the ATMD layout presented here can meet the control performances required for the considered practical case.

A final point which deserves attention is related to those cases in which the ATMD main structure (the cantilever beam here) hosting the piezoelectric elements is replaced by any other structure showing non-negligible modal superimposition, or cases in which, even if the modes are initially spaced in frequency, the adaptation leads to modes close in frequency. In these cases, the low modal superimposition hypothesis is not met anymore. This implies that the formulas presented above to link eigenfrequency and shunt capacitance values lose accuracy (e.g., Eq. (12)). On the one hand, one can still use the formulas above for a preliminary tuning of the capacitance value and then the perfect tuning can be obtained by implementing a control strategy on the real-time controller (see, e.g., [57]). The other possibility is to improve the description of the link between eigenfrequency and capacitance values by a multi-degree-of-freedom estimation approach, instead of the single-degree-of-freedom approach used so far. Such a multi-degree-of-freedom approach, which is based on Eqs. (2) and (3), is presented in Appendix C.

7. Conclusion

This paper has shown that it is possible to design and build multi-mode adaptive tuned mass dampers based on a cantilever beam and piezoelectric shunt. The piezoelectric elements have to be shunted to impedances made of negative/positive capacitances. This

Table A.7
Symbols used in the paper.

Symbol	Meaning
P	Number of piezoelectric patches
y	Displacement of the constraint
t	Time
U	Transverse displacement of the beam
x	Coordinate along the beam
N	Number of modes
$\boldsymbol{\Phi}_i$	ith mode shape normalised to unit modal mass and with all patches short-circuited
q_i	ith modal coordinate
ω_i	ith eigenfrequency with all patches short-circuited
ξ_i	ith non-dimensional damping ratio with all patches short-circuited
F_i	ith modal force
$\chi_{i,p}$	Coupling coefficient for mode i and patch p
V_p	Voltage between the electrodes of the pth patch
C_{∞},p	Blocked capacitance value for the pth patch
$C_{0,p}$	Capacitance value for the pth patch at the null frequency
$C_{i,p}$	Modal capacitance for the pth patch and ith mode
Q_p	Charge in one electrode of the pth patch
Ω	Angular frequency
$k_{i,p}$	Modal electro-mechanical coupling factor for mode i and patch p
$\omega_{i,p}^{\mathrm{oc}}$	ith eigenfrequency with the pth patch open-circuited
$C_{\mathrm{a},p}$	Shunt capacitance for the pth patch
n	Number of eigenfrequencies to be tuned
$\omega_{i,\mathrm{new}}$	New value of the ith eigenfrequency achieved with the shunt
R_p	Shunt resistance for the pth patch
$\hat{C}$	Capacitance of the circuit used to develop an NC
$R_{\mathrm{e},1}$, $R_{\mathrm{e},2}$, $\hat{R}$	Resistances of the circuit used to develop an NC
s	Laplace operator
[I]	Identity matrix
$a, b, c, \Delta_i, \lambda, A_i, B_i, D_i, X_{i,p}, r_i, \alpha_p, \beta_p, \tilde{R}, R_{\mathrm{eq}}$, [S], [Θ], [Ṡ], T_1, T_2, T_3	Symbols derived from the quantities above

device is able to independently act on a number of eigenfrequencies equal to the number of piezoelectric elements used, thus allowing for tuning them on those of a primary system undergoing different shifts of its eigenfrequencies.

Analytical formulas have been given for linking the values of the capacitances used in the shunt impedances to the resulting eigenfrequency values, and vice versa, also addressing the stability of the electro-mechanical system. The adaptation area can be strongly increased by using negative capacitances closer and closer to the stability limits. Nevertheless, it was found that large areas can be covered staying far away from instability and choosing the position of the piezoelectric elements such that a given piezoelectric bender is strongly coupled to one of the modes whose eigenfrequency has to be shifted.

The theoretical outcomes were successfully validated through an experimental campaign with a cantilever beam equipped with two piezoelectric elements.

CRediT authorship contribution statement

S. Manzoni: Conceptualization, Formal analysis, Investigation, Methodology, Resources, Supervision, Validation, Visualization, Writing – original draft, Writing – review & editing. **M. Berardengo:** Conceptualization, Formal analysis, Investigation, Methodology, Supervision, Validation, Writing – review & editing. **F. Boccuto:** Data curation, Formal analysis, Investigation, Software, Validation, Writing – review & editing. **M. Vanali:** Data curation, Visualization.

Declaration of competing interest

The authors declare that they have no known competing financial interests or personal relationships that could have appeared to influence the work reported in this paper.

Data availability

Data will be made available on request.

Appendix A. Symbols used in the paper

Table A.7 presents the meaning of the symbols used in the paper.

Appendix B. Stability conditions

Relying on Eqs. (21) to (24), to assure stability of the ith mode, A_i, B_i and D_i must have the same sign. Furthermore, for the stability of the whole system, all the modes must be stable. This appendix addresses the problem of finding these stability conditions.

The constants A_i and B_i are positive if the terms $(C_{\mathrm{a},p=1}+C_{i,p=1})$ and $(C_{\mathrm{a},p=2}+C_{i,p=2})$ have the same sign, and negative if they have opposite sign. Therefore, to find stability, four different situations must be addressed considering the sign of the constant D_i:

1. if $(C_{\mathrm{a},p=1}+C_{i,p=1})$ and $(C_{\mathrm{a},p=2}+C_{i,p=2})$ are both negative, then D_i must be positive (configuration 1, named conf1);
2. if $(C_{\mathrm{a},p=1}+C_{i,p=1})$ and $(C_{\mathrm{a},p=2}+C_{i,p=2})$ are both positive, then D_i must be positive (configuration 2, named conf2);
3. if $(C_{\mathrm{a},p=1}+C_{i,p=1})$ is positive and $(C_{\mathrm{a},p=2}+C_{i,p=2})$ is negative, then D_i must be negative (configuration 3, named conf3);
4. if $(C_{\mathrm{a},p=1}+C_{i,p=1})$ is negative and $(C_{\mathrm{a},p=2}+C_{i,p=2})$ is positive, then D_i must be negative (configuration 4, named conf4).

All these possible cases are discussed in the next subsections.

As mentioned in Section 3.2, in investigating the stability conditions, the starting points considered here are the stability conditions when a single piezoelectric element is connected to an NC and the other is short-circuited. According to [55] and relying on Eq. (25), these conditions are

$$C_{\mathrm{a},p} > -C_{i,p} \tag{B.1}$$

or

$$C_{\mathrm{a},p} < -C_{i-1,p} \tag{B.2}$$

when considering only the ith mode, and

$$C_{\mathrm{a},p} > -C_{\infty,p} \tag{B.3}$$

or

$$C_{\mathrm{a},p} < -C_{0,p} \tag{B.4}$$

for the whole system (i.e., considering all the modes, which means that these are the actual stability conditions of the electromechanical system).

B.1. Configuration 1

The first configuration leads to the following computations. Since $(C_{\mathrm{a},p=1}+C_{i,p=1})$ and $(C_{\mathrm{a},p=2}+C_{i,p=2})$ are both negative, then:

$$C_{\mathrm{a},p=1} < -C_{i,p=1},\quad C_{\mathrm{a},p=2} < -C_{i,p=2} \tag{B.5}$$

According to [55], the relationship between $C_{i-1,p}$ and $C_{i,p}$ is:

$$C_{i-1,p} = C_{i,p}(1+k_{i,p}^2) \tag{B.6}$$

Thus, according to Eq. (B.6), the conditions in Eq. (B.5) are less restrictive compared to the stability conditions valid in case of using a single NC (see Eq. (B.2)). Therefore, the conditions in Eq. (B.5) are changed to

$$C_{\mathrm{a},p=1} < -C_{i-1,p=1},\quad C_{\mathrm{a},p=2} < -C_{i-1,p=2} \tag{B.7}$$

The requirement of a positive value for D_i (see Eq. (24)) leads to:

$$C_{\mathrm{a},p=2}\left[\chi_{i,p=1}^2+\omega_i^2(C_{\mathrm{a},p=1}+C_{i,p=1})\right] > -\chi_{i,p=1}^2 C_{i,p=2} - (\chi_{i,p=2}^2+\omega_i^2 C_{i,p=2})(C_{\mathrm{a},p=1}+C_{i,p=1}) \tag{B.8}$$

According to Eqs. (6) and (B.6), the term $\chi_{i,p=1}^2+\omega_i^2(C_{\mathrm{a},p=1}+C_{i,p=1})$ can be rearranged as:

$$\chi_{i,p=1}^2+\omega_i^2(C_{\mathrm{a},p=1}+C_{i,p=1}) = \omega_i^2(C_{\mathrm{a},p=1}+C_{i-1,p=1}) \tag{B.9}$$

which is negative because of Eq. (B.7). Thus, the inequality in Eq. (B.8) becomes:

$$C_{\mathrm{a},p=2} < -C_{i,p=2}(1+k_{i,p=2}^2 X_{i,p=1}) \tag{B.10}$$

where

$$X_{i,p=1} = \frac{C_{\mathrm{a},p=1}+C_{i,p=1}}{C_{\mathrm{a},p=1}+C_{i-1,p=1}} = \frac{C_{\mathrm{a},p=1}+C_{i,p=1}}{C_{\mathrm{a},p=1}+C_{i,p=1}(1+k_{i,p=1}^2)} \tag{B.11}$$

According to Eqs. (B.6) and (B.7), $X_{i,p=1} \geq 1$ and, thus, Eq. (B.10) is more restrictive than the condition on $C_{\mathrm{a},p=2}$ in Eq. (B.7). Therefore, the stability conditions for the ith mode for conf1 are:

$$C_{\mathrm{a},p=1} < -C_{i-1,p=1}, \quad C_{\mathrm{a},p=2} < -C_{i,p=2}(1 + k^2_{i,p=2} X_{i,p=1}) \tag{B.12}$$

If all the modes of the coupled system are now considered, the conditions in Eq. (B.12) must be met for all of them. Relying on Eq. (25), the strictest cases are those for the low-order modes, which are characterised by the largest values of $C_{i,p=2}$. However, the value of $X_{i,p=1}$ depends also on that of $k^2_{i,p=1}$ (see Eq. (B.11)) and, thus, the actual mode with the strictest condition related to the second inequality in Eq. (B.12) (i.e., the inequality in Eq. (B.10)) changes case by case. However, for the sake of simplicity, it is possible to assume here that the first mode is that with the strictest stability condition related to Eq. (B.10) and, thus, the global stability condition becomes that provided in Eq. (26).

It is noticed that isolating $C_{\mathrm{a},p=1}$ in place of $C_{\mathrm{a},p=2}$ in Eq. (B.8), the stability conditions become:

$$C_{\mathrm{a},p=2} < -C_{i-1,p=2}, \quad C_{\mathrm{a},p=1} < -C_{i,p=1}(1 + k^2_{i,p=1} X_{i,p=2}) \tag{B.13}$$

These stability conditions are equivalent to the conditions of Eq. (B.12). Considering that the conditions in Eq. (B.13) msut be met for all the modes, the resulting stability conditions for the global coupled system are those provided in Eq. (28).

Therefore, finally, the stability conditions for conf1 are those provided in Eq. (26), or in Eq. (28) equivalently.

B.2. Configuration 2

Since $(C_{\mathrm{a},p=1} + C_{i,p=1})$ and $(C_{\mathrm{a},p=2} + C_{i,p=2})$ are both positive, then $C_{\mathrm{a},p=1} > -C_{i,p=1}$ and $C_{\mathrm{a},p=2} > -C_{i,p=2}$. With these conditions (which already satisfy the conditions related to the use of a single NC), D_i is always positive (see Eq. (24)). If all the modes of the coupled system are now considered, the conditions $C_{\mathrm{a},p=1} > -C_{i,p=1}$ and $C_{\mathrm{a},p=2} > -C_{i,p=2}$ must be fulfilled for all of them. According to Eq. (25), the strictest case is that for the mode of highest order and, thus, the stability conditions related to conf2 are those provided in Eq. (29).

B.3. Configurations 3 and 4

Using an approach similar to those already discussed in Appendices B.1 and B.2, the following stability conditions are found, also noticing that, as mentioned in Section 3.2, no conditions less restrictive than those related to the use of a single NC are accepted here. Considering only the ith mode, the obtained stability conditions for conf3 are:

$$C_{\mathrm{a},p=1} > -C_{i,p=1}, \quad C_{\mathrm{a},p=2} < -C_{i-1,p=2} \tag{B.14}$$

For conf4, the obtained stability conditions are:

$$C_{\mathrm{a},p=1} < -C_{i-1,p=1}, \quad C_{\mathrm{a},p=2} > -C_{i,p=2} \tag{B.15}$$

When considering all the modes of the electro-mechanical system, the conditions of conf3 become those in Eq. (30), while the conditions for conf4 become those in Eq. (31).

Appendix C. Multi-degree-of-freedom estimation approach

According to Eqs. (2) and (3) and to the definition of the modal capacitance, and assuming to consider the hth and $(h+1)$th modes which have to be tuned with two patches, the following equations can be written:

$$\ddot{q}_i + 2\xi_i \omega_i \dot{q}_i + \omega_i^2 q_i - \sum_{p=1}^{P} \chi_{i,p} V_p = F_i \qquad \forall\, i = h, h+1 \tag{C.1}$$

$$C_{(h+1),p} V_p - Q_p + \sum_{i=h}^{h+1} \chi_{i,p} q_i = 0 \qquad \forall\, p = 1, 2 \tag{C.2}$$

Considering the relationship between V_p and Q_p due to a shunt capacitance, Q_p can be eliminated from Eq. (C.2), thus writing V_p as a function of the modal coordinates. Then, through this expression, Eq. (C.1) can be written as function only of the modal coordinates, eliminating V_p. The resulting equations are:

$$\begin{aligned} &\ddot{q}_h + 2\xi_h \omega_h \dot{q}_h + \omega_h^2 q_h + \chi_{h,p=1}(\chi_{h,p=1} q_h + \chi_{(h+1),p=1} q_{(h+1)})/(C_{\mathrm{a},p=1} + C_{(h+1),p=1}) \\ &\quad + \chi_{h,p=2}(\chi_{h,p=2} q_h + \chi_{(h+1),p=2} q_{(h+1)})/(C_{\mathrm{a},p=2} + C_{(h+1),p=2}) = F_h \end{aligned} \tag{C.3}$$

$$\begin{aligned} &\ddot{q}_{(h+1)} + 2\xi_{(h+1)} \omega_{(h+1)} \dot{q}_{(h+1)} + \omega_{(h+1)}^2 q_{(h+1)} + \chi_{(h+1),p=1}(\chi_{h,p=1} q_h + \chi_{(h+1),p=1} q_{(h+1)})/(C_{\mathrm{a},p=1} + C_{(h+1),p=1}) \\ &\quad + \chi_{(h+1),p=2}(\chi_{h,p=2} q_h + \chi_{(h+1),p=2} q_{(h+1)})/(C_{\mathrm{a},p=2} + C_{(h+1),p=2}) = F_{(h+1)} \end{aligned} \tag{C.4}$$

These equations can be written in matrix form as:

$$[\dot{S}] = [\Theta][S] + [F_h, 0, F_{(h+1)}, 0]^{\mathrm{T}} \tag{C.5}$$

where the superscript T indicates the transposed matrix and:

$$[\mathrm{S}] = [\dot{q}_h, q_h, \dot{q}_{(h+1)}, q_{(h+1)}]^{\mathrm{T}} \tag{C.6}$$

$$[\dot{\mathrm{S}}] = [\ddot{q}_h, \dot{q}_h, \ddot{q}_{(h+1)}, \dot{q}_{(h+1)}]^{\mathrm{T}} \tag{C.7}$$

$$[\Theta] = \begin{bmatrix} -2\xi_h\omega_h & T_1 & 0 & T_2 \\ 1 & 0 & 0 & 0 \\ 0 & T_2 & -2\xi_{(h+1)}\omega_{(h+1)} & T_3 \\ 0 & 0 & 1 & 0 \end{bmatrix} \tag{C.8}$$

and

$$T_1 = -\omega_h^2 - \frac{\chi_{h,p=1}^2}{C_{\mathrm{a},p=1} + C_{(h+1),p=1}} - \frac{\chi_{h,p=2}^2}{C_{\mathrm{a},p=2} + C_{(h+1),p=2}} \tag{C.9}$$

$$T_2 = -\frac{\chi_{h,p=1}\chi_{(h+1),p=1}}{C_{\mathrm{a},p=1} + C_{(h+1),p=1}} - \frac{\chi_{h,p=2}\chi_{(h+1),p=2}}{C_{\mathrm{a},p=2} + C_{(h+1),p=2}} \tag{C.10}$$

$$T_3 = -\omega_{(h+1)}^2 - \frac{\chi_{(h+1),p=1}^2}{C_{\mathrm{a},p=1} + C_{(h+1),p=1}} - \frac{\chi_{(h+1),p=2}^2}{C_{\mathrm{a},p=2} + C_{(h+1),p=2}} \tag{C.11}$$

Moving to the Laplace domain, the eigenvalues of the system can be found solving the following equation for s:

$$\det(s[\mathrm{I}] - [\Theta]) = 0 \tag{C.12}$$

being [I] the identity matrix. Finally, from the obtained eigenvalues, the corresponding eigenfrequencies can be calculated.

It is noticed that in case there are modes close to the hth and $(h+1)$th, they can be taken into consideration in the above equations to account also for their influence. Similarly, two non-subsequent modes can be considered for the control action and the modes between the two of them can be added in the above model to account for their influence.

References

[1] S. Krenk, Frequency analysis of the tuned mass damper, J. Appl. Mech. 72 (6) (2005) 936–942.
[2] N. Hoang, Y. Fujino, P. Warnitchai, Optimal tuned mass damper for seismic applications and practical design formulas, Eng. Struct. 30 (3) (2008) 707–715, http://dx.doi.org/10.1016/j.engstruct.2007.05.007.
[3] S. Krenk, J. Høgsberg, Equal modal damping design for a family of resonant vibration control formats, J. Appl. Mech. 19 (9) (2013) 1294–1315.
[4] K. Lievens, G. Lombaert, K. Van Nimmen, G. De Roeck, P. Van den Broeck, Robust vibration serviceability assessment of footbridges subjected to pedestrian excitation: Strategy and applications, Eng. Struct. 171 (June) (2018) 236–246, http://dx.doi.org/10.1016/j.engstruct.2018.05.047.
[5] L. Wang, S. Nagarajaiah, Y. Zhou, W. Shi, Experimental study on adaptive-passive tuned mass damper with variable stiffness for vertical human-induced vibration control, Eng. Struct. 280 (2023) 115714, http://dx.doi.org/10.1016/j.engstruct.2023.115714.
[6] X. Lu, Q. Zhang, W. Wu, J. Shan, Data-Driven Two-Level Performance Evaluation of Eddy-Current Tuned Mass Damper for Building Structures Using Shaking Table and Field Testing, Comput.-Aided Civ. Infrastruct. Eng. 34 (1) (2019) 38–57, http://dx.doi.org/10.1111/mice.12373.
[7] S. Li, W. Gao, D. Yurchenko, X. Wang, J. Wang, X. Liu, Novel spacer-tuned-mass-damper system for controlling vibrations of hangers, Mech. Syst. Signal Process. 167 (Part A) (2022) 108537, http://dx.doi.org/10.1016/j.ymssp.2021.108537.
[8] X. Su, H. Kang, T. Guo, Modelling and energy transfer in the coupled nonlinear response of a 1:1 internally resonant cable system with a tuned mass damper, Mech. Syst. Signal Process. 162 (May 2021) (2021) 108058, http://dx.doi.org/10.1016/j.ymssp.2021.108058.
[9] M. Khazaee, S.E. Khadem, A. Moslemi, A. Abdollahi, A comparative study on optimization of multiple essentially nonlinear isolators attached to a pipe conveying fluid, Mech. Syst. Signal Process. 141 (2020) 106442, http://dx.doi.org/10.1016/j.ymssp.2019.106442.
[10] S. Li, H. Li, L. Zhang, X. Wang, A comparative study of isolation performance of electric automobile seat's suspension added by negative-stiffness structure models, Noise Vib. Worldwide 54 (2–3) (2023) 81–91, http://dx.doi.org/10.1177/0957456523115424.
[11] G.M. Chatziathanasiou, N.A. Chrysochoidis, D.A. Saravanos, Autonomous Semi-Active Tuned Mass Damper for Adaptive Vibration Control of Aircraft Structures, AIAA Sci. Technol. Forum Exposit AIAA SciTech Forum 2022 (2022) 1–12, http://dx.doi.org/10.2514/6.2022-1342.
[12] W. Ma, X. Jin, J. Yu, Y. Yang, X. Liu, R. Shen, Oppositely oriented series multiple tuned mass dampers and application on a parallel machine tool, Mech. Syst. Signal Process. 163 (May 2021) (2022) 108196, http://dx.doi.org/10.1016/j.ymssp.2021.108196.
[13] P. Wang, J. Chen, Nonlinear rotational inertial double-tuned mass damper for reducing human-induced floor vibration with frequency detuning, Mech. Syst. Signal Process. 172 (January) (2022) 109016, http://dx.doi.org/10.1016/j.ymssp.2022.109016.
[14] M. Yamamoto, T. Sone, Behavior of active mass damper (AMD) installed in high-rise building during 2011 earthquake off Pacific coast of Tohoku and verification of regenerating system of AMD based on monitoring, Struct. Control Health Monit. (21) (2014) 634–647, http://dx.doi.org/10.1002/stc.1590.
[15] K. Zhou, Q.-S. Li, X. Li, Dynamic Behavior of Supertall Building with Active Control System during Super Typhoon Mangkhut, J. Struct. Eng. 146 (5) (2020) 04020077, http://dx.doi.org/10.1061/(asce)st.1943-541x.0002626.
[16] L. Zhang, L. Hong, J.S. Dhupia, S. Johnson, Z. Qaiser, Z. Zhou, A novel semi-active tuned mass damper with a continuously tunable stiffness, Proc. Inst. Mech. Eng. C 237 (2023) 281–293, http://dx.doi.org/10.1177/09544062221119925.
[17] M. Brennan, Actuators for active control-tunable resonant devices, Appl. Mech. Eng. 5 (1) (2000) 63–74.
[18] E. Rustighi, M.J. Brennan, B.R. Mace, A shape memory alloy adaptive tuned vibration absorber: Design and implementation, Smart Mater. Struct. 14 (1) (2005) 19–28, http://dx.doi.org/10.1088/0964-1726/14/1/002.
[19] M. Berardengo, G. Della Porta, S. Manzoni, M. Vanali, A multi-modal adaptive tuned mass damper based on shape memory alloys, J. Intell. Mater. Syst. Struct. 30 (4) (2019) 536–555, http://dx.doi.org/10.1177/1045389X18818388.
[20] S. Manzoni, A. Argentino, F. Lucà, M. Berardengo, M. Vanali, SMA-based adaptive tuned mass dampers: Analysis and comparison, Mech. Syst. Signal Process. 186 (2023) 109883, http://dx.doi.org/10.1016/j.ymssp.2022.109883.
[21] F. Weber, C. Boston, M. Maślanka, An adaptive tuned mass damper based on the emulation of positive and negative stiffness with an MR damper, Smart Mater. Struct. 20 (1) (2011) 015012, http://dx.doi.org/10.1088/0964-1726/20/1/015012.

[22] F. Weber, M. Maślanka, Frequency and damping adaptation of a TMD with controlled MR damper, Smart Mater. Struct. 21 (5) (2012) 055011, http://dx.doi.org/10.1088/0964-1726/21/5/055011.
[23] S.B. Kumbhar, S.P. Chavan, S.S. Gawade, Adaptive tuned vibration absorber based on magnetorheological elastomer-shape memory alloy composite, Mech. Syst. Signal Process. 100 (2018) 208–223, http://dx.doi.org/10.1016/j.ymssp.2017.07.027.
[24] M. Acar, C. Yilmaz, Design of an adaptive–passive dynamic vibration absorber composed of a string–mass system equipped with negative stiffness tension adjusting mechanism, J. Sound Vib. 332 (2) (2013) 231–245, http://dx.doi.org/10.1016/j.jsv.2005.01.018.
[25] T. Long, M.J. Brennan, S.J. Elliott, Design of smart machinery installations to reduce transmitted vibrations by adaptive modification of internal forces, Proc. Instit. Mech. Eng. Part I: J. Syst. Control Eng. 212 (3) (1998) 215–228, http://dx.doi.org/10.1243/0959651981539415.
[26] J. Chen, C.T. Georgakis, Tuned rolling-ball dampers for vibration control in wind turbines, J. Sound Vib. 332 (21) (2013) 5271–5282, http://dx.doi.org/10.1016/j.jsv.2013.05.019.
[27] N. Carpineto, W. Lacarbonara, F. Vestroni, Hysteretic tuned mass dampers for structural vibration mitigation, J. Sound Vib. 333 (5) (2014) 1302–1318, http://dx.doi.org/10.1016/j.jsv.2013.10.010.
[28] Z.H. Wang, Y.W. Xu, H. Gao, Z.Q. Chen, K. Xu, S.B. Zhao, Vibration control of a stay cable with a rotary electromagnetic inertial mass damper, Smart Struct. Syst. 23 (6) (2019) 627–639, http://dx.doi.org/10.12989/sss.2019.23.6.627.
[29] Y. Xiang, P. Tan, H. He, H. Yao, X. Zheng, K. Yang, A novel bi-directional rail variable friction pendulum-tuned mass damper (BRVFP-TMD), Mech. Syst. Signal Process. 197 (April) (2023) 110396, http://dx.doi.org/10.1016/j.ymssp.2023.110396.
[30] C.L. Davis, G.A. Lesieutre, Actively tuned solid-state vibration absorber using capacitive shunting of piezoelectric stiffness, J. Sound Vib. 232 (3) (2000) 601–617, http://dx.doi.org/10.1006/jsvi.1999.2755.
[31] M. Lallart, L. Yan, Y.-C. Wu, D. Guyomar, Electromechanical semi-passive nonlinear tuned mass damper for efficient vibration damping, J. Sound Vib. 332 (22) (2013) 5696–5709, http://dx.doi.org/10.1016/j.jsv.2013.06.006.
[32] B. Bao, W. Tang, Semi-active vibration control featuring a self-sensing SSDV approach, Meas. J. Int. Meas. Confederat. 104 (2017) 192–203, http://dx.doi.org/10.1016/j.measurement.2017.03.018.
[33] R. Darleux, B. Lossouarn, J.-F. Deü, Passive self-tuning inductor for piezoelectric shunt damping considering temperature variations, J. Sound Vib. 432 (2018) 105–118.
[34] J. Toftekær, J. Høgsberg, Multi-mode piezoelectric shunt damping with residual mode correction by evaluation of modal charge and voltage, J. Intell. Mater. Syst. Struct. 31 (4) (2019) 570–586.
[35] Z.A. Shami, C. Giraud-Audine, O. Thomas, A nonlinear piezoelectric shunt absorber with a 2:1 internal resonance: Theory, Mech. Syst. Signal Process. 170 (2022) 108768, http://dx.doi.org/10.1016/j.ymssp.2021.108768.
[36] G. Konda Rodrigues, P. Gardonio, L. Dal Bo, E. Turco, Piezoelectric patch vibration control unit connected to a self-tuning RL-shunt set to maximise electric power absorption, J. Sound Vib. 536 (2022) 117154, http://dx.doi.org/10.1016/j.jsv.2022.117154.
[37] O. Heuss, R. Solloum, D. Mayer, T. Melz, Tuning of a vibration absorber with shunted piezoelectric transducers, Arch. Appl. Mech. 86 (2016) 1715–1732.
[38] G.M. Chatziathanasiou, N.A. Chrysochoidis, D.A. Saravanos, A semi-active shunted piezoelectric tuned mass damper for robust vibration control, J. Vib. Control 28 (2022) 2969–2983, http://dx.doi.org/10.1177/10775463211026487.
[39] G.M. Chatziathanasiou, N.A. Chrysochoidis, C.S. Rekatsinas, D.A. Saravanos, A semi-active shunted piezoelectric tuned-mass-damper for multi-modal vibration control of large flexible structures, J. Sound Vib. 537 (2022) 117222, http://dx.doi.org/10.1016/j.jsv.2022.117222.
[40] K. Yamada, T. Asami, Passive vibration suppression using 2-degree-of-freedom vibration absorber consisting of a beam and piezoelectric elements, J. Sound Vib. 532 (January) (2022) 116997, http://dx.doi.org/10.1016/j.jsv.2022.116997.
[41] K. Dekemele, P. Van Torre, M. Loccufier, Design, construction and experimental performance of a nonlinear energy sink in mitigating multi-modal vibrations, J. Sound Vib. 473 (2020) 115243, http://dx.doi.org/10.1016/j.jsv.2020.115243.
[42] G. Raze, J. Dietrich, G. Kerschen, Passive control of multiple structural resonances with piezoelectric vibration absorbers, J. Sound Vib. 515 (August) (2021) 116490, http://dx.doi.org/10.1016/j.jsv.2021.116490.
[43] Y.-W. Xu, Z.-D. Xu, R.-L. Zhao, Z.-H. Wang, Y. Li, C. Zhu, Multimode vibration control of stay cables using pseudo negative stiffness MR damping system, J. Intell. Mater. Syst. Struct. (2023) http://dx.doi.org/10.1177/1045389X221147958, (in press).
[44] O. Thomas, J.-F. Deü, J. Ducarne, Vibration of an elastic structure with shunted piezoelectric patches: Efficient finite-element formulation and electromechanical coupling coefficients, Internat. J. Numer. Methods Engrg. 80 (2) (2009) 235–268.
[45] J. Ducarne, O. Thomas, J. Deü, Placement and dimension optimization of shunted piezoelectric patches for vibration reduction, J. Sound Vib. 331 (14) (2012) 3286–3303.
[46] O. Thomas, J. Ducarne, J. Deü, Performance of piezoelectric shunts for vibration reduction, Smart Mater. Struct. 21 (1) (2012) 015008.
[47] M. Berardengo, S. Manzoni, J. Høgsberg, M. Vanali, Vibration control with piezoelectric elements: The indirect measurement of the modal capacitance and coupling factor, Mech. Syst. Signal Process. 151 (2021) 107350, http://dx.doi.org/10.1016/j.ymssp.2020.107350.
[48] L. Meirovitch, Fundamentals of Vibrations, McGraw-Hill, New York, 2001.
[49] J.-S. Wu, T.-L. Lin, Free vibration analysis of a uniform cantilever beam with point masses by an analytical-and-numerical-combined method, J. Sound Vib. 136 (2) (1990) 201–213, http://dx.doi.org/10.1016/0022-460X(90)90851-P.
[50] A. Ghasemi, M. Heidari-Rarani, B. Heidari-Sheibani, A. Tabatabaeian, Free transverse vibration analysis of laminated composite beams with arbitrary number of concentrated masses, Arch. Appl. Mech. 91 (6) (2021) 2393–2402, http://dx.doi.org/10.1007/s00419-021-01924-2.
[51] F. Cheli, G. Diana, Advanced Dynamics of Mechanical Systems, Springer, 2015.
[52] J. Høgsberg, Vibration control by piezoelectric proof-mass absorber with resistive-inductive shunt, Mech. Adv. Mater. Struct. 28 (2) (2021) 141–153, http://dx.doi.org/10.1080/15376494.2018.1551587.
[53] M. Berardengo, S. Manzoni, O. Thomas, C. Giraud-Audine, L. Drago, S. Marelli, M. Vanali, The reduction of operational amplifier electrical outputs to improve piezoelectric shunts with negative capacitance, J. Sound Vib. 506 (2021) 116163, http://dx.doi.org/10.1016/j.jsv.2021.116163.
[54] B. de Marneffe, A. Preumont, Vibration damping with negative capacitance shunts: Theory and experiment, Smart Mater. Struct. 17 (3) (2008) 035015.
[55] M. Berardengo, O. Thomas, C. Giraud-Audine, S. Manzoni, Improved resistive shunt by means of negative capacitance: New circuit, performances and multi mode control, Smart Mater. Struct. 25 (2016) 075033.
[56] B. Lossouarn, L. Rouleau, R. Darleux, J.-F. Deü, Comparison of passive damping treatments based on constrained viscoelastic layers and multi-resonant piezoelectric networks, J. Struct. Dyn. (1) (2021) 30–48, http://dx.doi.org/10.25518/2684-6500.63.
[57] M. Berardengo, A. Cigada, F. Guanziroli, S. Manzoni, Modelling and control of an adaptive tuned mass damper based on shape memory alloys and eddy currents, J. Sound Vib. 349 (2015) 18–38, http://dx.doi.org/10.1016/j.jsv.2015.03.036.
[58] M. Auleley, O. Thomas, C. Giraud-Audine, H. Mahé, Enhancement of a dynamic vibration absorber by means of an electromagnetic shunt, J. Intell. Mater. Syst. Struct. 32 (3) (2021) 331–354, http://dx.doi.org/10.1177/1045389X20957097.
[59] O. Thomas, C. Touzé, A. Chaigne, Asymmetric non-linear forced vibrations of free-edge circular plates. part II: Experiments, J. Sound Vib. 265 (5) (2003) 1075–1101.
[60] S. Behrens, A.J. Fleming, S.O.R. Moheimani, A broadband controller for shunt piezoelectric damping of structural vibration, Smart Mater. Struct. 12 (1) (2003) 18–28.
[61] S. Schleiter, O. Altay, Identification and semi-active control of structures with abrupt stiffness degradations, Mech. Syst. Signal Process. 163 (February 2021) (2022) 108131, http://dx.doi.org/10.1016/j.ymssp.2021.108131.